Development/Plasticity/Repair

Antagonistic Activities of Fmn2 and ADF Regulate Axonal F-Actin Patch Dynamics and the Initiation of Collateral Branching

Tanushree Kundu, Sooraj Siva Das, Lisas K. Sewatkar, Divya S. Kumar, Dhriti Nagar, and Aurnab Ghose
Indian Institute of Science Education and Research (IISER) Pune, Pune 411008, India

Interstitial collateral branching of axons is a critical component in the development of functional neural circuits. Axon collateral branches are established through a series of cellular processes initiated by the development of a specialized, focal F-actin network in axons. The formation, maintenance and remodeling of this F-actin patch is critical for the initiation of axonal protrusions that are subsequently consolidated to form a collateral branch. However, the mechanisms regulating F-actin patch dynamics are poorly understood. Fmn2 is a formin family member implicated in multiple neurodevelopmental disorders. We find that Fmn2 regulates the initiation of axon collateral protrusions in chick spinal neurons and in zebrafish motor neurons. Fmn2 localizes to the protrusion-initiating axonal F-actin patches and regulates the lifetime and size of these F-actin networks. The F-actin nucleation activity of Fmn2 is necessary for F-actin patch stability but not for initiating patch formation. We show that Fmn2 insulates the F-actin patches from disassembly by the actin-depolymerizing factor, ADF, and promotes long-lived, larger patches that are competent to initiate axonal protrusions. The regulation of axonal branching can contribute to the neurodevelopmental pathologies associated with Fmn2 and the dynamic antagonism between Fmn2 and ADF may represent a general mechanism of formin-dependent protection of Arp2/3-initiated F-actin networks from disassembly.

Key words: **ADF; axon collateral branching; cytoskeleton; F-actin patch; Fmn2; formins**

Significance Statement

Axonal branching is a key process in the development of functional circuits and neural plasticity. Axon collateral branching is initiated by the elaboration of F-actin filaments from discrete axonal F-actin networks. We show that the neurodevelopmental disorder-associated formin, Fmn2, is a critical regulator of axon collateral branching. Fmn2 localizes to the collateral branch-inducing F-actin patches in axons and regulates the stability of these actin networks. The F-actin nucleation activity of Fmn2 protects the patches from ADF-mediated disassembly. Opposing activities of Fmn2 and ADF exert a dynamic regulatory control on axon collateral branch initiation and may underly the neurodevelopmental defects associated with Fmn2.

Introduction

Axonal branching is a key component in the establishment of functional neuronal circuits during development and recovery following injury. The process allows a single neuron to make multiple synaptic contacts and is critical for the development of accurate connectivity, structural plasticity and state-dependent recruitment of neuronal groups (Low and Cheng, 2006; Gibson and Ma, 2011; Kalil and Dent, 2014; Armijo-Weingart and Gallo, 2017; Rockland, 2018).

A major mechanism of axonal branching involves the development of interstitial collateral branches. The process of generating axon collaterals is a multistep process involving both extrinsic and intrinsic cues (Katz, 1985; Chalmers et al., 2016; Armijo-Weingart and Gallo, 2017; Menon and Gupton, 2018). Collaterals which appear *de novo* from the axon shaft can be induced by extracellular cues, such as netrin1 (Dent et al., 2004; Lebrand et al., 2004) nerve growth factor (NGF; Gallo and Letourneau, 1998), and brain-derived growth factor (BDNF; Danzer et al., 2002; Marler et al., 2008). On the other hand, factors such as semaphorin 3A (Dent et al., 2004) and slit1a (Campbell et al., 2007) act locally to suppress branch

Received Dec. 11, 2020; revised Aug. 17, 2022; accepted Aug. 22, 2022.

Author contributions: T.K. and A.G. designed research; T.K., S.S.D., D.S.K., L.K.S., and D.N. performed research; T.K., S.S.D., D.S.K., and A.G. analyzed data; T.K. wrote the first draft of the paper; S.S.D., D.S.K., L.K.S., and A.G. edited the paper; A.G. wrote the paper.

T.K. was supported by a University Grants Commission fellowship. D.N. was supported by a Council of Scientific and Industrial Research fellowship. The NFGFHD at IISER Pune is supported by a grant from the Department of Biotechnology, Government of India (BT/INF/22/SP17358/2016). We thank Dr. N. K. Subhedar, Indian Institute of Science Education and Research (IISER) Pune for his critical reading of this manuscript. We acknowledge the IISER Pune Microscopy Facility and the National Facility for Gene Function in Health and Disease (NFGFHD) at IISER Pune for access to equipment and infrastructure. The study was aided by intramural support from IISER Pune and a grant from the Council of Scientific and Industrial Research, Government of India (37(1689)/17/EMR-II) to A.G.

The authors declare no competing financial interests.

Correspondence should be addressed to Aurnab Ghose at aurnab@iiserpune.ac.in.

https://doi.org/10.1523/JNEUROSCI.3107-20.2022

formation. These cues trigger downstream signal transduction pathways, which impinge on the underlying cytoskeletal dynamics to form a branch.

The process of axonal branching begins with the formation of a focal F-actin patch (Gallo, 2006; Orlova et al., 2007; Ketschek and Gallo, 2010; Andersen et al., 2011). These transient patches are a spontaneous accumulation of branched actin mainly regulated by the WAVE1 activated Arp2/3 complex that nucleates branched actin filaments (Spillane et al., 2012). Only a small proportion of these patches forms an axonal protrusion (Orlova et al., 2007; Ketschek and Gallo, 2010; Armijo-Weingart and Gallo, 2017). The proposed model for the conversion of a patch into a protrusion involves the convergence of branched actin filaments which are rapidly extended by the activities actin elongators such as Ena/VASP proteins and formins (Yang and Svitkina, 2011; Armijo-Weingart and Gallo, 2017). Other activities involve bundling of extending F-actin filaments, membrane remodeling and finally consolidation by microtubule invasion. While the Ena/VASP family of proteins has been demonstrated to promote collateral branching (Dwivedy et al., 2007), not much is known about the function of formins in the generation of axonal protrusions to initiate collateral branching (Kawabata Galbraith and Kengaku, 2019).

Fmn2 is expressed in the developing and the mature nervous systems across vertebrate phyla (Leader and Leder, 2000; Dutta and Maiti, 2015; Sahasrabudhe et al., 2016; Nagar et al., 2021). While Fmn2 has been implicated in neurodevelopmental disorders, intellectual disability, age-related dementia, microcephaly and corpus callosum agenesis in humans (Perrone et al., 2012; Almuqbil et al., 2013; Law et al., 2014; Agís-Balboa et al., 2017; Anazi et al., 2017; Marco et al., 2018; Gorukmez et al., 2020), its function in neurons is only recently being discovered. At the neuronal growth cone, Fmn2 regulates filopodial dynamics and stability of adhesion complexes to mediate axonal outgrowth (Sahasrabudhe et al., 2016; Ghate et al., 2020). Fmn2 also regulates microtubule dynamics and influences growth cone turning (Kundu et al., 2021). Further, Fmn2 may influence dendritic spine density in hippocampal neurons (Law et al., 2014).

In this study, we identify a novel role for Fmn2 in initiating axon collateral branches. We show that Fmn2 is critical for the maintenance and stability of that F-actin patches that generate axonal protrusions. This specialized axonal F-actin network is protected from disassembly by actin depolymerizing factor (ADF) by Fmn2-mediated F-actin assembly.

Materials and Methods

Culturing primary neurons

Spinal cord tissue from stage HH 25–26 (day 5–6) chick (*Gallus gallus*) embryos of either sex (Venkateshwara hatcheries Ltd.) were dissected out in L-15 medium (Invitrogen, HiMedia) with added 1× penstrep (Invitrogen). After dissection, the tissue was trypsinized (0.05% Trypsin-EDTA (Lonza, HiMedia) at 37°C for 15–20 min and then resuspended in Optimem (Invitrogen) before cuvette-based electroporation (CUY21SC, Nepagene). The transfected neurons were plated on glass-bottomed 35 mm plastic dishes and incubated at 37°C for 24–36 h in L-15 medium with 10% fetal bovine serum (FBS; Invitrogen) and 1× penstrep (Invitrogen). The dishes were coated with poly-L-lysine (1 mg/ml; Sigma) and laminin (20 µg/ml; Sigma) before plating.

Transfection with plasmids and morpholinos

The details of the plasmids used in this study are given in Table 1. Fmn2 was knocked down in cultured neurons using translation-blocking anti-gFmn2 morpholinos (Fmn2-MO; 5′-CCATCTTGATTCCCCATGATTTTTC-3′; 100 µM). Standard control morpholino (Ctl-MO; 5′-CCTCTTACCTCAGTTACAATTTATA-3′) was used as a negative control. These reagents have been extensively characterized for knock-down efficiency and specificity (Sahasrabudhe et al., 2016; Ghate et al., 2020). For fixed experiments, the neurons were co-transfected with pCAG-GFP and Ctl-MO or Fmn2-MO. Correspondingly, for live-imaging experiments, pCAG-tractin-GFP was used in place of pCAG-GFP. Rescue experiments were performed with triple transfections of pCAG-GFP + Fmn2-MO + mCherry-tagged constructs.

For fixed analysis of Fmn2 overexpression experiments, pCAG-gFmn2-GFP was co-transfected with either pCAG-mCherry or with pCAG-ADF S3A-mCherry. For live-imaging of Fmn2 overexpression, pCAG-tractin-GFP was co-transfected with either pCAG-mCherry or gFmn2-mCherry or gFmn2-mCherry+ ADF S3A mCherry.

Immunofluorescence

For quantifying branching, the neurons were fixed in 4% paraformaldehyde, 0.25% glutaraldehyde in PHEM buffer [60 mM PIPES (Sigma), 25 mM HEPES (Sigma), 10 mM EGTA (Sigma), and 4 mM $MgSO_4{\cdot}7H_2O$)]. After 10 min of permeabilization in 0.2% triton-PHEM, blocking was done with 3% BSA for 1 h at room temperature (RT). The primary antibody for total microtubule (anti-α-tubulin, DM1a, Sigma) was used at a concentration of 1:2000 and incubated at 4°C overnight. Anti-mouse Alexa 405 secondary antibodies at 1:1500 dilution and incubated for 1 h was used for signal detection. Phalloidin-633 (Invitrogen; 1:250) or Phalloidin-568 (Invitrogen; 1:150) was used to label F-actin before mounting in MOWIOL-DABCO [2.5% 1, 4-diazabicyclo-octane (DABCO; Sigma), 10% MOWIOL 4-88 (Sigma), 25% glycerol (Sigma), and 0.1 M Tris-HCl; pH 8.5]. For endogenous Fmn2 staining, neurons were fixed with 4% paraformaldehyde and 0.25% glutaraldehyde in 1× PBS buffer for 20 min at 37°C. After permeabilization with 0.1% Triton X-100/PBS for 30 min at RT, blocking was done with 3% BSA in 1× PBS buffer for 1 h at RT. Primary antibody Fmn2 antisera (anti-CRQ; Sahasrabudhe et al., 2016) was used at a concentration of 1:3000 overnight at 4°C. The anti-rabbit 488 secondary was used at a concentration of 1:2000 for 2 h at RT.

Zebrafish maintenance, morpholino injections, and imaging procedures

The protocols used in this study were approved by the Institutional Animal Ethics Committee and the Institutional Biosafety Committee of Indian Institute of Science Education and Research (IISER) Pune.

Adult zebrafish (*Danio rerio*) were housed in an aquarium with circulating water at 28.5°C, pH in the range of 7.2–7.8 and conductivity below 500 siemens. A 14/10 h light/dark cycle was maintained. The transgenic line Tg(mnx1:GFP) (Flanagan-Steet et al., 2005) was used for all experiments. Zebrafish embryos, of either sex, obtained by crossing the wild-type zebrafish were injected at 1 cell stage with 2 nl morpholino solution (0.125 mM) as indicated and raised in embryo medium (E3) at 28.5°C until 22 and 48 h postfertilization (hpf). The morpholinos used were obtained from Gene Tools Inc. and have been previously described and validated (Kundu et al., 2021; Nagar et al., 2021). The sequences of the morpholinos are as given below.

Standard Ctl-MO:

5′-CCTCTTACCTCAGTTACAATTTATA-3′.

Splice-blocking Fmn2 morpholino (Zf-Fmn2_MO):

5′-ACAGAAGCGGTCATTACTTTTTGGT-3′.

The morpholino injected Tg(mnx1:GFP) embryos at 22 and 48 hpf were imaged after mounting in coverslip bottom 35 mm dishes using low melt point agarose (Sigma) supplemented with 0.003% MS-222 (Sigma). The laterally mounted embryos were imaged on the inverted LSM 780 confocal microscope (Zeiss) with a 25× oil immersion objective (NA 1.4). The quantification of motor neuron branching was done using the NeuronJ plugin of Fiji.

Imaging

The fixed images were acquired using Zeiss LSM 710, 780 or Leica SP8 confocal systems with a 63×, 1.4 NA oil or 100×, 1.4 NA oil objective.

Live-imaging of actin patches was done in widefield mode on the Olympus IX-81 system (Olympus Corporation) with 100×, 1.4 NA Apo

Table 1. Plasmid constructs used in this study indicating source, vector backbone, cloning strategy and primers used for cloning

Plasmid name	Plasmid backbone	Insert name	Source	GenBank accession number	Primer used for cloning	Region cloned and cloning strategy
pCAG-GFP	pCAG	—	Addgene (11500)	—	—	—
pCAG-mCherry	pCAG	mCherry	This study	—	Fwd 5′-ATATATACCGGTCGCCACCATGGT GAGCAAGGGCGAGGAGG-3′ Rev 5′-ATATATGCGGCCGCTTTACTTGTAC AGCTCGTCCATGCCGCC-3′	Cloned by ligation between AgeI and NotI sites
pCAG-Tractin-GFP/ mCherry	pCAG-GFP and pCAG-mCherry	F-tractin	This study	NM_031045.2	Fwd 5′-ATGGCGCGACCACGGGGCGC GGGGCCCTGCAGCCCCGGGTTGGA GCGGGCTCCGCGCCGGAGCGTCGG GGAGCTG-3′ Rev 5′-CCCCCTGCGGCCGCTGCGGCGG CGACTGCGGCGCAGCGCGCTTCG AAGAGCAGGCGCAGCTCCCCGAC GCTCCGG-3′	1–113, cloned by homologous recombination for between Age1 and Kpn1
pCAG-gFmn2-GFP/ mCherry	pCAG-GFP and pCAG-mCherry	gFmn2	Previously generated by A. Jacob in the corresponding author's laboratory.	KU711529.1	NA	Complete cds, cloned by homologous recombination using SmaI
pCAG-mFmn2-FL-GFP/ mCherry	pCAG-GFP and pCAG-mCherry	mFmn2; gift from Dr. Philip Leder, Harvard Medical School	This study	NM_019445	Fwd 5′-AGTCGACGGTACCCGCCACCATGG GGAACCAGGATGGGAAG-3′ Rev 5′-GGTGGCGACCGGTGGATCCCGGGt CGTTTTCATGCTTATCTTCGCTTTAAT C -3′	complete cds, cloned By homologous recombination between KpnI and XmaI
pCAG-mFmn2-ΔFSI-GFP/ mCherry	pCAG-GFP and pCAG-mCherry	pCAGmFmn2-FL	This study	NM_019445	Fwd 5′-GCAAAGAATTCTGCAGTCGACGGT ACCCGCCACCATGGGGAACCAGGAT GG 3′ Rev 5′-CCATGGTGGCGACCGGTGGATCCC GGGCCTTCTGCCTACACACCTCC-3′	1–4662, cloned by homologous recombination between KpnI and XmaI
pCAG-mFmn2-I2A-GFP/ mCherry	pCAG-GFP and pCAG-mCherry	pCAGmFmn2-FL	This study	NM_019445	Fwd 5′-CAAAAGGTCACAAGCAGTAGGAG CTCTAATGTCTAGTCTGCATTT AGATATG-3′ Rev 5′-CATATCTAAATGCAGACTAGACATT AGAGCTCCTACTGCTTGTGACCT TTTG-3′	Mutation I1226A, cloned by homologous recombination between KpnI and XmaI
pCAG-ADF S3E-GFP/ mCherry	pCAG-GFP and pCAG-mCherry	ADF S3E, cDNA gifted by Dr. J. Bamburg, Colorado State University	This study	—	Fwd 5′-ATTTTGGCAAAGAATTCCACCGCCAT GGCAGAAGGAGTACAAG-3′ Rev 5′-CTTTTGAAGGAAGTCCTGTGgCCCG GGATCCACCGGTCGC-3′	Complete cds, cloned by homologous recombination between Age1 and Kpn1
pCAG-ADF S3A-GFP/ mCherry	pCAG-GFP and pCAG-mCherry	ADF S3A, cDNA gifted by Dr. J. Bamburg, Colorado State University	This study	—	Fwd 5′-ATTCTGCAGTCGACGGTAC-3′ Rev TCACCATGGTGGCGACCGGTGGATC CCCCACAGGACTTCCTTCAAA AGC-3′	Complete cds, cloned by homologous recombination between Age1 and Kpn1

oil immersion objective and Hamamatsu ORCA-R2 CCD camera. The temperature was maintained at 37°C in a humid chamber for the duration of imaging. Time-lapse images of Tractin-GFP were acquired using the RT Xcellence software with a time interval of 2 s for 150 frames.

For colocalization of Fmn2 and actin, imaging was done using the Oxford Nanoimager system with HILO (High Inclination and Laminated Optical sheet) setup using the 100× 1.4 NA objective. Dual-color images were acquired with 500-ms time interval for 600 frames at 37°C.

Image analysis

For quantification of protrusion density, the entire axon was considered, excluding the growth cone and the soma. Protrusions ≥0.5 μm were

considered for analysis. The first frame of each tractin-GFP time-lapse movie was used to calculate the patch area and density. The area of a F-actin patch was measured manually using the freehand selection tool after background subtraction. For calculating patch area of patches that formed protrusions, the area of the patch one frame before a detectable protrusion was observed, was taken into consideration. For patch lifetime analysis, the time-lapse images were drift corrected using the StackReg plugin of ImageJ followed by generation of kymographs using the KymoClear 2.0 plugin. Segmented lines were drawn manually on each kymograph to mark the patches. Patch lifetime was calculated using the velocity-measurement tool plugin. For calculating the lifetime of patches that gave rise to a protrusion, the patches were tracked manually from the first frame of detectable appearance to the last frame of disappearance. For colocalization analysis, ROIs of actin patches were identified using the tractin channel. Then, fluorescence of every ROI in both the channels was quantified using the formula, corrected fluorescence (CTCF) = integrated density – (area of selected cell X mean fluorescence of background readings). The fluorescence values of both the channels were plotted in X-Y table in Prism 8 to calculate Pearson's correlation coefficient and r^2 values. All analysis was performed after anonymizing the genotype.

Statistical analysis and graphical representation

All the graphical representation and statistical analyses were performed using GraphPad Prism 8. Graphical representations were plotted using scatter dot plot with middle line showing the mean and error bars indicating the SEM. Mann–Whitney *U* test was employed for two groups and for multiple comparisons Kruskal–Wallis test was done followed by uncorrected Dunn's test as indicated in each figure. To compare frequency distributions the Kolmogorov–Smirnov test was used. Number of data points quantified in each graph and the biological replicates have been indicated in the figure legends.

Ethics approval and data availability

All protocols used in this study were approved by Institutional Animal Ethics Committee and the Institutional Biosafety Committee of IISER Pune. All data generated or analyzed during this study are included in this published article. The raw data are available from the corresponding author on reasonable request.

Results

Fmn2 promotes initiation of axon collateral branching in spinal neurons

Formins are involved in neuronal growth and axon guidance during development (Kawabata Galbraith and Kengaku, 2019). Several formin family members localize to growth cone filopodia and regulate filopodial dynamics (Barzik et al., 2014; Szikora et al., 2017; Rama et al., 2018). The F-actin nucleation/elongation function of formins are also implicated in the dynamics of axonal actin "hotspots" (Ganguly et al., 2015). Fmn2 function in growth cones is necessary for axonal outgrowth and growth cone filopodial stability (Sahasrabudhe et al., 2016; Ghate et al., 2020). As a majority of axon collateral branches arise from a filopodia-like protrusion from the axonal shaft, we investigated whether the formin, Fmn2, was involved on axon collateral branching.

To evaluate the role of Fmn2 in axonal branching, Fmn2 was depleted in chick spinal neurons using well-characterized, specific translation-blocking morpholinos targeting Fmn2 (Fmn2-MO; see Materials and Methods). Phalloidin staining of F-actin (Fig. 1*A*,*B*) revealed a drastic reduction of collateral axonal protrusions (Fig. 1*C*) in neurons transfected with Fmn2-MO (0.118 ± 0.016 protrusions/μm) compared with Ctl-MO transfected neurons (0.193 ± 0.02 protrusions/μm).

Conversely, the overexpression of GFP-tagged chick Fmn2 (gFmn2-GFP; Fig. 1*D*,*E*) doubled the frequency of protrusions (0.246 ± 0.022 protrusions/μm; Fig. 1*E*,*F*) as compared with control GFP-expressing neurons (0.128 ± 0.015 protrusions/μm; Fig. 1*D*,*F*).

To observe axonal collateral formation, live-imaging was undertaken with neurons transfected with the GFP-tagged F-actin probe, F-tractin (trac-GFP; Fig. 1*G*). As reported earlier (Orlova et al., 2007; Ketschek and Gallo, 2010; Andersen et al., 2011), axon collateral branching was preceded with the emergence and elaboration of a juxta-membrane F-actin patch. The F-actin patch, extended into the membrane protrusion to initiate collateral branching. Time-lapse tracking of F-tractin in Fmn2 depleted axons revealed a significantly reduced frequency of branch initiation (0.013 ± 0.003 protrusions/μm/min; Fig. 1*H*) compared with Ctl-MO co-transfected axons (0.027 ± 0.004 protrusions/μm/min; Fig. 1*H*). Conversely, F-tractin-tagged axons overexpressing mCherry-tagged chick Fmn2 (gFmn2-mCh) exhibited a significantly higher rate of branch initiation (0.076 ± 0.009 protrusions/μm/min; Fig. 1*I*) than axons overexpressing mCherry (0.038 ± 0.013 protrusions/μm/min; Fig. 1*I*). The live imaging experiments allow us to identify Fmn2 function in protrusion initiation rather than other function, like stabilizing existing protrusions.

Thus, Fmn2 protein expression dynamically regulates the initiation of axon collateral branching in spinal neurons and highlights a novel developmental function for Fmn2 in neuronal development.

Fmn2 regulates the formation of axon collateral branches

To evaluate the role of Fmn2 in regulating axon collateral branching *in vivo*, we depleted the zebrafish ortholog of Fmn2 using well-characterized morpholinos (Kundu et al., 2021; Nagar et al., 2021) in a transgenic fish line expressing GFP in the primary motor neurons. We evaluted the axon collateral branching of the caudal primary (CaP) motor neuron at 22 and 48 hpf. At 22 hpf, collateral branching was reduced by almost half (0.445 ± 0.0315 branches/μm in Ctl-MO and 0.244 ± 0.0256 branches/μm in zFmn2-MO condition; Fig. 2*A*–*C*). Similarly, at 48 hpf the collateral branching of the CaP motor neurons was also significantly reduced (0.335 ± 0.0380 branches/μm in Ctl-MO and 0.126 ± 0.0095 branches/μm in zFmn2-MO condition; Fig. 2*D*–*F*). These data demonstrate the function of Fmn2 as a regulator of axon collateral branching *in vivo*.

As microtubule entry into protrusions is a late event indicative of the maturation of collateral branches, we scored collateral protrusions containing microtubules in chick spinal neurons to evaluate the role of Fmn2 in regulating mature branch formation. Compared with Ctl-MO treated controls (0.167 ± 0.033; Fig. 2*G*,*I*), transfection of Fmn2-MO resulted in a reduction the density of microtubule-containing collateral branches (0.079 ± 0.02; Fig. 2*H*,*I*). These data indicate that the reduction in axonal protrusions on Fmn2 depletion (Fig. 1*C*) translate to reduced number of mature collateral branches.

Collectively, the data implicate Fmn2 as a key regulator of axon collateral branching *in vivo* and indicate that reduced protrusion initiation observed on Fmn2 depletion persist as deficits in mature branch numbers.

Fmn2 localizes to the base of axonal protrusions and colocalizes with actin patches

Immunostaining of endogenous Fmn2 revealed the accumulation of Fmn2 in chevron-shaped structures at the axonal membrane at the base of axonal protrusions (Fig. 3*A*) in a pattern suggestive of its role in branch development. Co-expression of tagged gFmn2 and F-tractin also revealed the accumulation of

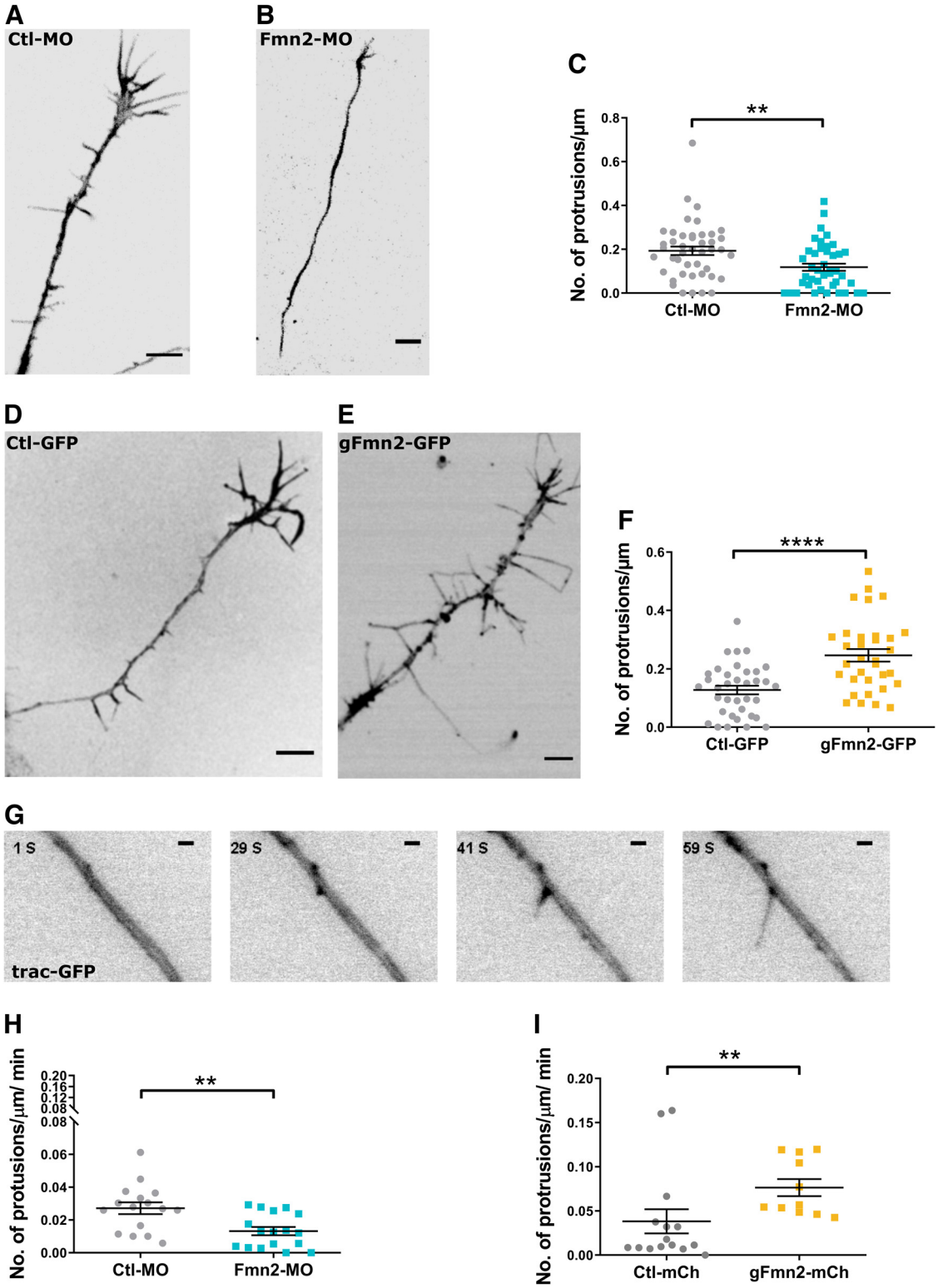

Figure 1. Fmn2 promotes collateral protrusions in axons by increasing the rate of branch formation. Representative images of neuron with collateral protrusions after co-transfection of either Ctl-MO (***A***) or Fmn2-MO (***B***) and pCAG-GFP. The neurons were fixed and stained with phalloidin after 24 h of incubation. ***C***, Graphical representation of the number of protrusions (Ctl-MO, $n = 44$ and Fmn2-MO, $n = 42$; $p = 0.003$). ***D***, ***E***, Representative phalloidin-stained micrographs of collateral protrusions in GFP-overexpressing and gFmn2-GFP-overexpressing neurons 24 h after transfection. ***F***, Graphical representation of the number of protrusions (GFP, $n = 36$ and gFmn2-GFP $n = 33$; $p < 0.0001$). ***G***, Four frames from a time-lapse recording of the development of a collateral protrusion from a F-actin patch. Tractin-GFP (trac-GFP) was used to label F-actin (S, second). ***H***, Quantification of the frequency of new protrusion formation in in morpholino-treated neurons (Ctl-MO, $n = 16$ axons; Fmn2-MO, $n = 17$ axons; $p = 0.004$). ***I***, Frequency of protrusion initiation in Fmn2/GFP-overexpressing neurons (Ctl-GFP, $n = 15$ axons; Fmn2-GFP, $n = 11$ axons; $p = 0.004$). The data are obtained from at least three independent experiments. All the values were plotted with the mean ± SEM indicated. Data were analyzed using the two-tailed Mann–Whitney *U* test; $^{**}p < 0.01$; $^{****}p < 0.0001$. Scale bar: 10 µm (***A***, ***B***, ***D***, ***E***) and 1 µm (***G***).

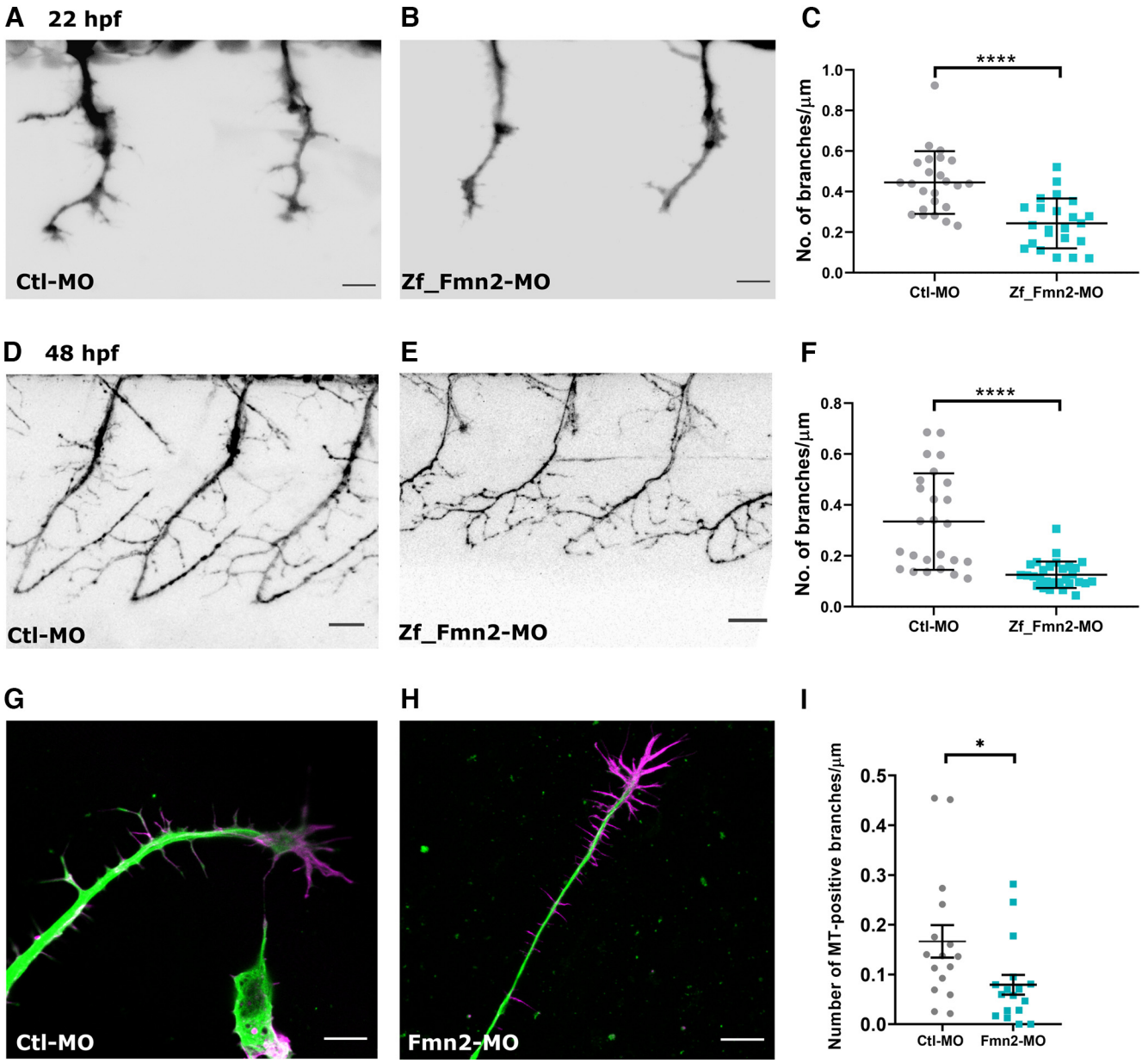

Figure 2. Fmn2 is required for the development of mature axonal branches *in vivo* and *in vitro*. Representative micrographs of *mnx1*:GFP-labeled spinal neurons in zebrafish larvae injected with control (Ctl-MO; ***A***, ***D***) and Fmn2-morphopholinos (Zf_Fmn2-MO; ***B***, ***E***) at stage 22 hpf (***A***, ***B***) and at 48 hpf (***D***, ***E***), respectively. ***C***, Quantification of branching density *in vivo* at 22 hpf (Ctl-MO, $n = 24$ and Zf_Fmn2-MO, $n = 23$ neurons; ****$p < 0.0001$). ***F***, Quantification of branching density at 48 hpf (Ctl-MO, $n = 25$ and Zf_Fmn2-MO $n = 30$ neurons; ****$p < 0.0001$). The values are plotted as mean and SEM, and data were analyzed using the Mann–Whitney *U* test and obtained from at least three independent experiments. Representative images of chick spinal neurons co-transfected with pCAG-GFP and either Ctl-MO (***G***) or chick Fmn2-MO (***H***). The neurons were fixed and stained with phalloidin and anti-tubulin antibodies after 36 h of incubation. Scale bar: 10 µm. The quantification of the density of microtubule-containing branches is shown in ***I*** (Ctl-MO, $n = 16$ and Fmn2-MO, $n = 17$; $p = 0.0184$; *$p < 0.05$). The values are plotted as mean and SEM, and data were analyzed using the Mann–Whitney *U* test and obtained from two independent experiments.

Fmn2 in chevron-shaped structures at the axonal membrane base of axonal protrusions (Fig. 3*B*).

Time-lapse imaging of the axon shaft revealed the colocalization of Fmn2 to the developing axonal F-actin patch (marked by F-tractin) that could subsequently contribute to the generation of an axonal protrusion (Fig. 3*E*). Following the development of the protrusion, Fmn2 remained accumulated at the base of the protrusion for several minutes after the branch had been initiated.

In order to evaluate how long after the initiation of collateral branching, starting with the initiation of a protrusion, was Fmn2 retained at the base of branches we evaluated the localization of Fmn2 at the base of mature branches using the presence of microtubules as an indicator maturation. These experiments revealed that a majority of (63%) microtubule-containing branches had Fmn2 accumulation at their base (Fig. 3*C*). Interestingly, the length of collateral branches not having Fmn2 at their bases was more than those that had Fmn2 persisting at their bases (8.323 ± 0.6399 µm with no Fmn2 at the base compared with the mean length of 5.525 ± 0.4468 µm with Fmn2 presence at the base; Fig. 3*D*). These data suggest while Fmn2 is involved in the early stages of branch initiation, as branches mature (presence of microtubule) and grow (increase in length), Fmn2 at their bases is no longer necessary. This observation is consistent with cryoelectron tomographic observations of a dense actin network at the base of nascent branches,

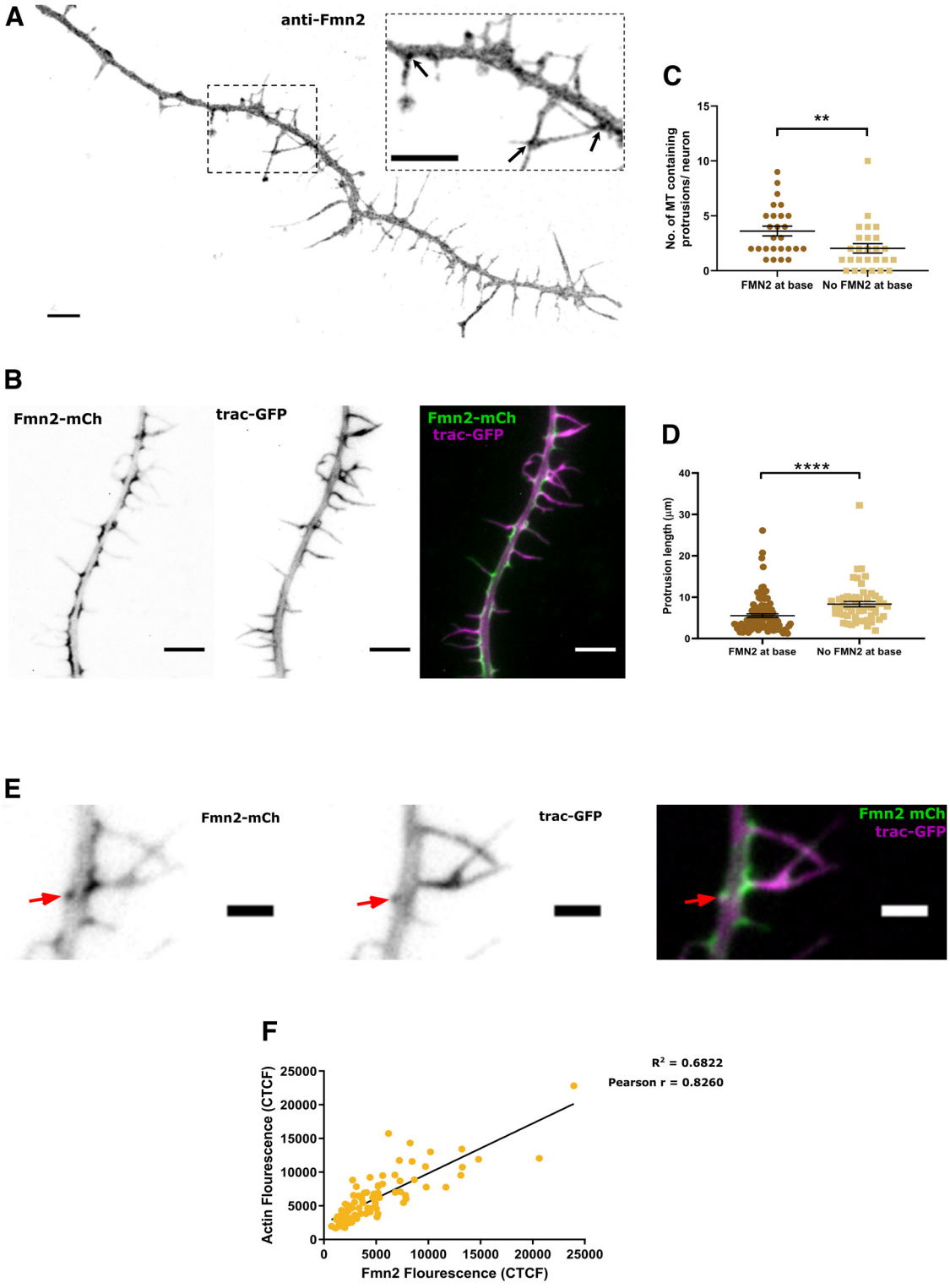

Figure 3. Fmn2 accumulates at the base of early protrusions and colocalizes with the protrusion forming F-actin patches in the axon. ***A***, Representative confocal micrograph showing the distribution of endogenous Fmn2 along the axons of chick spinal neurons. Inset shows a magnified image of the boxed region. Arrows point to the localization of Fmn2 at the base of branches. Scale bar: 10 μm. ***B***, Representative micrographs of Fmn2-mCherry (Fmn2-mCh; grayscale in the left-most panel and green in the right-most panel) and F-tractin-GFP (trac-GFP; grayscale in the middle panel and magenta in the right-most panel) and the overlay of the two channels. Fmn2 forms chevron-shaped structure at the base of axonal protrusions. ***C***, Number of total protrusions that contain microtubules with or without Fmn2 localized at the base ($n = 27$ neurons; $^{**}p < 0.01$) and their length distribution (***D***; $n = 94$ for Fmn2 at base and $n = 55$ for no Fmn2 at base; $^{****}p < 0.0001$). ***E***, Representative micrographs from dual-color time-lapse imaging showing Fmn2-mCherry (Fmn2-mCh; grayscale in the left-most panel and green in the right-most panel) and F-tractin-GFP (trac-GFP; grayscale in the middle panel and magenta in the right-most panel) and the overlay of the two channels. Red arrow indicates the F-actin colocalized with Fmn2, which eventually initiates a protrusion. Fmn2 was found to colocalize with F-actin patches and the colocalization is quantified in ***F***. The values are plotted as *XY* data points with a linear regression slope ($n = 86$; Pearson's correlation coefficient = 0.8260; $R^2 = 0.6822$; $p < 0.0001$). The data are from three biological replicates. CTCF, corrected total cell fluorescence. Scale bar: 10 μm (***A***), 2 μm (***B***), and 5 μm (***E***).

which is subsequently resolved as branches mature and elongate (Nedozralova et al., 2022).

Following the dynamics of Fmn2 and F-tractin by time-lapse imaging revealed an initial accumulation of Fmn2 at the membrane where a protrusion would be initiated at an average of 37.25 ± 11.2 s earlier than the appearance of an actin patch, which marked the location of initiation. 65% of all actin patches in the axon colocalized with Fmn2. However, all F-actin patches that gave rise to protrusions contained Fmn2 throughout their lifetime and increasing intensity of actin strongly correlated with Fmn2 intensity (Pearson correlation 0.82; $R^2 = 0.68$; Fig. 3*F*).

Fmn2 appears to be recruited to the membrane before the initiation of the F-actin patch and was subsequently found to be associated with actin patches generating protrusions. However, the accumulation of both actin and Fmn2 at the base of branches reduces as they mature and elongate. These data highlight a primary role of Fmn2 in the early, initial stages of branch formation.

Axonal F-actin patch dynamics, but not formation, is regulated by Fmn2

Axonal F-actin networks are expected to exist in a dynamic equilibrium between nucleation activities and depolymerizing activities. A proportion of axonal F-actin patches induce the development of axon collateral branches by initiating axonal protrusions. However, little is known about the dynamics of these axonal F-actin networks. To identify Fmn2 function in axonal F-actin patches, we dynamically visualized these networks used fluorophore-tagged F-tractin as a probe.

Neither Fmn2 depletion nor overexpression (both conditions that alter the extent of collateral branching) changed the density of F-actin patches in axons (Fig. 4*A*,*B*). While the above data suggested the lack of involvement of Fmn2 in initiating the formation of F-actin patches, the analysis of patch sizes revealed a positive correlation with the expression levels of Fmn2. The size of the F-actin patches was significantly reduced on Fmn2 depletion (0.152 ± 0.012 μm^2; Fig. 4*C*) compared with Ctl-Mo-treated neurons (0.181 ± 0.012 μm^2; Fig. 4*C*). On the other hand, compared with controls (0.135 ± 0.015 μm^2; Fig. 4*D*), overexpression of Fmn2 led to larger patch sizes (0.178 ± 0.011 μm^2; Fig. 4*D*).

We analyzed kymographs generated from the time-lapse images of tractin-GFP to assess the dynamics of the F-actin patches (Fig. 4*E*–*G*). Reduced levels of Fmn2 drastically shortened the lifetime of the F-actin patches from 53.6 0 ± 4.821 s in controls to 33.93 ± 2.136 s in Fmn2-MO transfected neurons (Fig. 4*F*,*H*). The analysis also revealed that Fmn2 knock-down resulted in multiple cycles of patch formation and disappearance occurring in the same region of the axon (Fig. 4*F*, red arrowheads), leading to a "blinking" phenomenon. This observation underscores the dynamic balance of F-actin patch assembly/disassembly and implicates Fmn2 in patch maintenance. The fact that the patch "blinks" at the same location suggests the presence of a nucleating core that is then elaborated by assembly promoting factors including Fmn2. Upon depletion of Fmn2, the balance shifts in favor of disassembly. Repeated nucleation is also suggestive of the lack of involvement of Fmn2 in F-actin patch initiation.

Overexpression of gFmn2 increased the F-actin patch lifetime (76.28 ± 4.477 s; Fig. 4*G*,*H*) compared with controls (34.65 ± 1.895 s; Fig. 4*G*,*H*), suggesting a stabilizing function.

Frequency distribution of patch lifetimes across 20-s bins also demonstrated that, relative to controls, the occurrence of short-lived patches was increased on Fmn2 depletion ($p < 0.0001$; Fig. 5*A*), while long-lived patches were enhanced on Fmn2 overexpression ($p < 0.0001$; Fig. 5*B*).

In order to relate patch sizes and lifetimes to the initiation of axonal collaterals, we compared these parameters between F-actin patches that result in axonal protrusion and to all patches. F-actin patches that subsequently resulted in an axonal protrusion were relatively larger and were long-lasting (Fig. 5*C*,*D*). In fact, the few patches that resulted in filopodia, despite Fmn2 knock-down, were comparable in size and lifetime with those initiating protrusions in controls (Fig. 5*E*,*F*).

Collectively, our data indicate the regulation of F-actin patch dynamics by Fmn2. F-actin patches need to elaborate to a competent size and lifetime before it can initiate an axonal protrusion. While not inducing patch formation, Fmn2 appears to be essential in the maintenance of F-actin patches allowing enough patches to reach protrusion initiation competence.

F-actin nucleation activity of Fmn2 is required for patch stability and branch initiation

In vitro studies have shown that Fmn2 nucleates F-actin filaments and facilitates elongation by barbed-end actin polymerization (Montaville et al., 2014, 2016). Data from the fly orthologue of Fmn2, *Cappuccino*, indicated that the mutation of a single isoleucine residue to alanine abrogated its F-actin nucleation/polymerization activity (Quinlan et al., 2007; Roth-Johnson et al., 2014). Sequence alignment revealed that this residue was conserved across taxa (Fig. 6*A*,*B*). We mutated this conserved isoleucine at position 1226 to alanine in mouse Fmn2 (mFmn2-IA). Mouse Fmn2 (mFmn2-FL) cDNA does not have the binding site for the translation-blocking morpholino's against chick Fmn2, thus mFmn2-FL and mFmn2-IA were co-expressed along with Fmn2-MO in rescue experiments to evaluate Fmn2 function.

Axonal branching was rescued with the expression of morpholino resistant full-length mFmn2 in morphant chick neurons (Fig. 6*C*,*E*). However, the nucleation deficient mutant of mouse Fmn2 (mFmn2-IA) failed to rescue the decrease in collateral branching (Fig. 6*D*,*E*). The reduction in F-actin patch area and lifetime in Fmn2 morphant axons were also rescued by co-expression of mFmn2-FL but the mFmn2-IA failed to rescue either of these F-actin patch parameters (Fig. 6*F*–*I*) with small, short-lived actin patches.

Taken together, the rescue experiments demonstrate that the nucleation activity of Fmn2 is required for regulating F-actin patch dynamics and consequently collateral branching.

Fmn2 and ADF act antagonistically to regulate actin patch stability and axonal branching

The F-actin patch "blinking" observed on depletion of Fmn2 suggested that axonal F-actin patches are dynamically balanced by stabilizing and destabilizing activities. With the identification of F-actin nucleation by Fmn2 in regulating F-actin patches, we sought to test this hypothesis directly. Formin nucleated F-actin is resistant to the actin depolymerizing activity of cofilin both *in vitro* and *in vivo* (Mizuno et al., 2018). Further, recent evidence implicates the ADF/cofilin family in regulating axon branching (Tedeschi et al., 2019). We tested whether Fmn2 maintains patch stability by antagonizing the depolymerizing activity of ADF (the ADF/cofilin family member in chick with highest depolymerizing activity; Chen et al., 2004).

Co-expression of a phospho-mimetic, inactive ADF (S3E), which functions as a dominant-negative mutant, along with Fmn2-MO was able to rescue the reduction in collateral protrusion

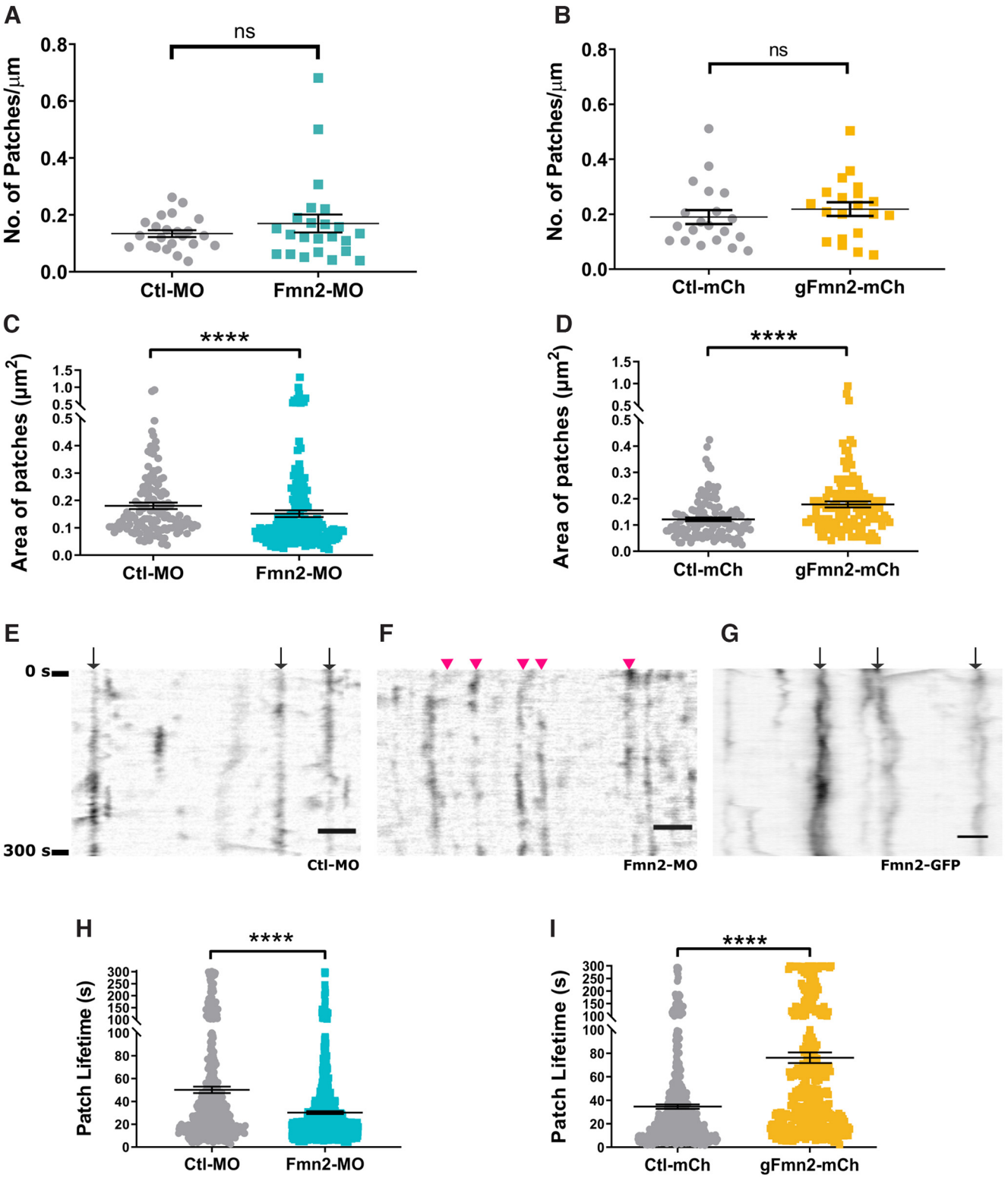

Figure 4. Fmn2 is necessary for patch stability but does not affect actin patch formation. ***A***, The density of F-actin patches in the entire axon is unchanged between Ctl-MO ($n = 23$ axons) and Fmn2-MO ($n = 23$ axons; $p = 0.8962$) transfected neurons. ***B***, Overexpression of mCherry-tagged chick Fmn2 (gFmn2-mCh; $n = 20$ axons) does not change the density of axonal F-actin patches compared with fluorophore (Ctl-mCh) expression neurons ($n = 20$ axons; $p = 0.3547$). ***C***, The area of axonal F-actin patches is lower in Fmn2-MO transfected neurons ($n = 189$ patches) compared with controls ($n = 128$ patches; $p < 0.0001$). Conversely, ***D***, Fmn2 overexpression (gFmn2-mCh; $n = 125$ patches; $p < 0.0001$) increases F-actin patch size relative to control neurons (Ctl-mCh; $n = 121$ patches). ***E–G***, Representative kymographs, from Ctl-MO (***E***), Fmn2-MO (***F***), and Fmn2-GFP (***G***) transfected neurons depicting F-actin patches lifetimes. Arrows mark actin patches and the pink arrow heads in ***F*** indicate the repeated appearance and disappearance "blinking" of the F-actin patch in the same location over time. The quantification of actin patch lifetimes is shown in ***H*** for Ctl-MO ($n = 490$) and Fmn2-MO ($n = 693$; $p < 0.0001$), and in ***I*** for mCherry (Ctl-mCh; $n = 576$) and Fmn2-mCherry (gFmn2-mCh; $n = 379$; $p < 0.0001$). The data are obtained from three independent experiments. All the values were plotted with the mean ± SEM indicated. The two-tailed Mann–Whitney *U* test was used as a test of significance. ns, $p > 0.05$, ****$p < 0.0001$. Scale bar: 2 μm.

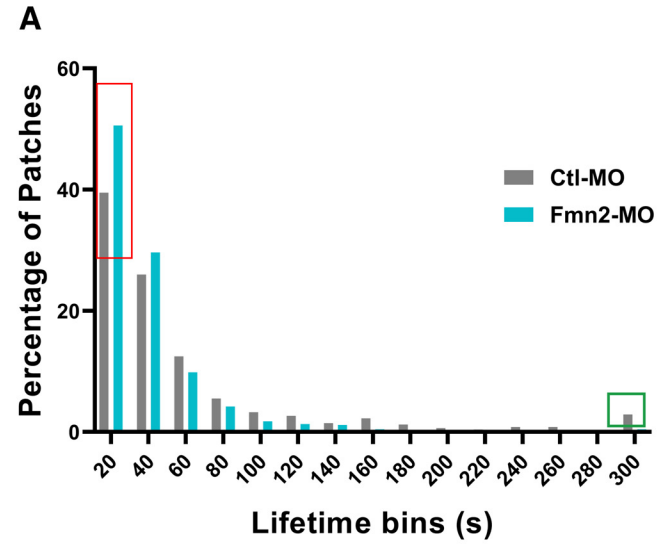

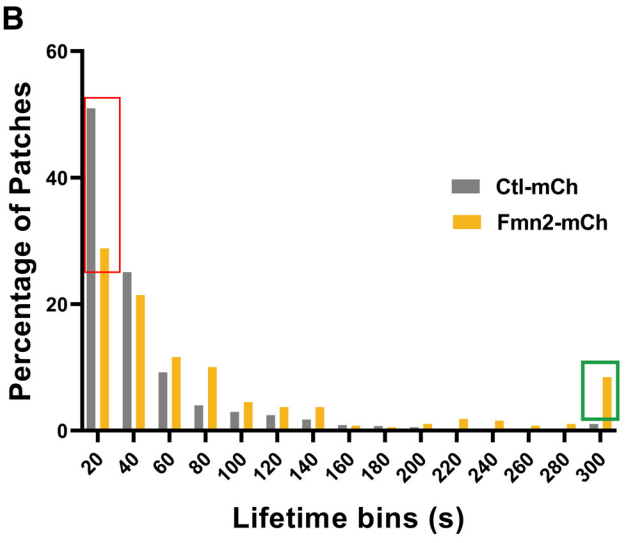

C

Treatment	Area of total no. of patches (μm²)	Area of patches that form protrusion (μm²)
Ctl-MO	0.1805± 0.012	0.2749± 0.038
Fmn2-MO	0.1519± 0.012	0.3073± 0.039

D

Treatment	Lifetime of total no. of patches (s)	Lifetime of patches that form protrusion (s)
Ctl-MO	50.10 ± 2.84	60.35 ± 10.71
Fmn2-MO	30.16 ± 1.29	64.13 ± 14.71

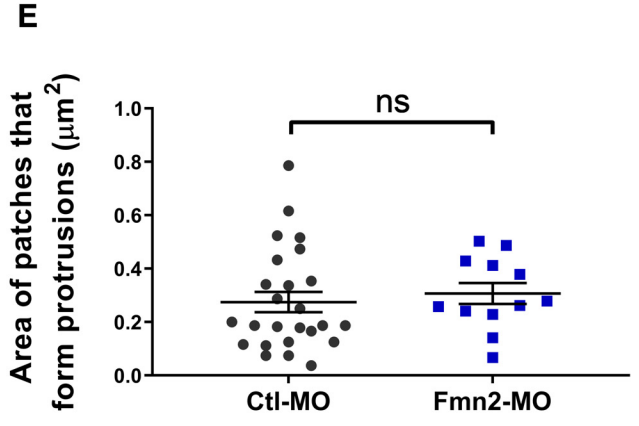

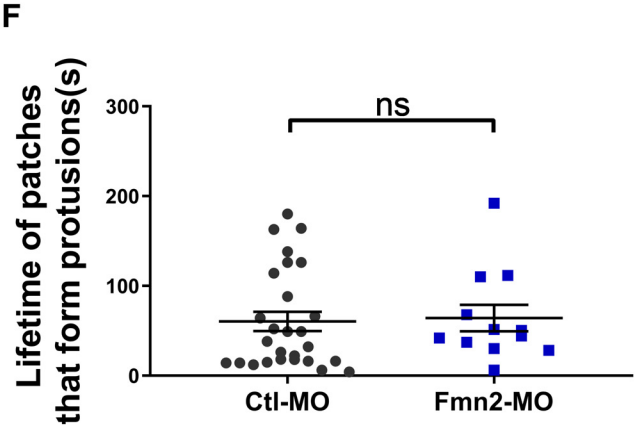

Figure 5. Fmn2 regulates F-actin patch lifetimes though patches giving rise to protrusions have comparable areas and lifetimes across treatments. ***A***, ***B***, Distribution of all actin patch lifetimes in 20-s bins across the 5 min of time-lapse imaging in Fmn2 depletion (Ctl-MO; $n = 490$ and Fmn2-MO; $n = 693$) and Fmn2 overexpression (Ctl-mCh; $n = 576$ and Fmn2-mCh; $n = 379$) conditions, respectively. The distribution shows that the largest proportion of patches exists for <20 s in all conditions. ***A***, Fmn2-MO treatment increases the proportion of short-lived patches (red box) compared with control-MO treatment ($p < 0.0001$; Kolmogorov–Smirnov test). ***B***, Overexpression of Fmn2 shifts patch lifetimes toward longer-lived patches (green box) while decreasing the proportion of short-lived patches (red box). A substantially higher proportion of patches last for the whole 5 min (green box) when Fmn2 is overexpressed ($p < 0.0001$; Kolmogorov–Smirnov test). ***C***, ***D***, Tables showing the mean patch area and patch lifetime of all the axonal patches and of patches that give rise to protrusions in Ctl-MO and Fmn2-MO transfected axons. Comparison of patch area (***E***) and patch lifetime (***F***) of patches that generate protrusions form filopodia in Ctl-MO-treated ($n = 25$ and 27, respectively) and Fmn2-MO-treated ($n = 12$; ns $p > 0.05$) neurons. Protrusion-generating actin patches have similar areas and lifetimes in Fmn2-depleted and control axons. Unless indicated otherwise, all the values are plotted as mean and SEM and data were analyzed using Mann–Whitney *U* test and obtained from at least three independent experiments. The data for the frequency distributions in ***A***, ***B*** were obtained from three independent experiments and were compared using the Kolmogorov–Smirnov test.

observed in axons depleted of Fmn2 (Fig. 7*A*). Conversely, co-expression of constitutively-active ADF (S3A) along with Fmn2-GFP suppressed the increased branching observed on Fmn2 overexpression (Fig. 7*B*).

Consistent with the rescue of branching, expression of the inactive ADF S3E was also able to rescue the reduction patch area and lifetime in Fmn2 morphants (Fig. 7*C*,*E*). Similarly, the expression of constitutively-active ADF S3A restored the Fmn2 overexpression-induced increased actin patch area and lifetime (Fig. 7*D*,*F*) to control levels.

Thus, a dynamic balance between Fmn2-mediated F-actin assembly and ADF-induced disassembly regulates the lifetime of axonal F-actin patches and, in turn, the development of axon collateral branches.

Discussion

Co-existence of functionally distinct cytoskeleton networks in the cytosol necessitates unique regulatory mechanisms that confer specific properties to these networks. The F-actin structures

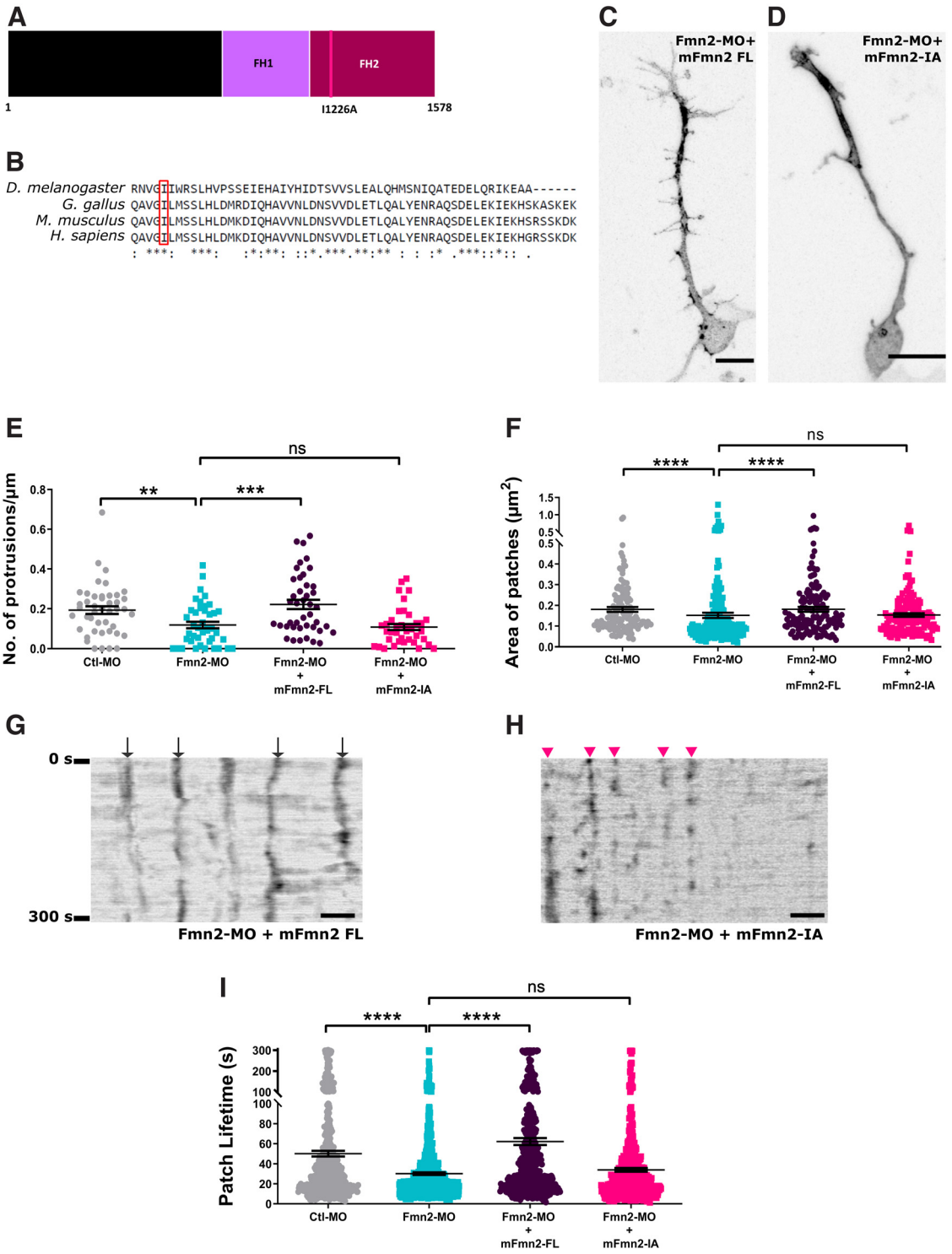

Figure 6. Actin nucleation activity of Fmn2 is necessary for the development of axonal protrusions and F-actin patch stability. ***A***, Schematic representation of domains of Fmn2 with the nucleation-dead mutation (I1226A) indicated in the FH2 domain. ***B***, Clustal-W multiple alignment of the FH2 domain of Fmn2 protein showing conservation of this critical amino acid (boxed) across phyla. ***C–E***, Representative micrographs of neurons with collateral protrusions co-expressing Fmn2-MO and GFP-tagged constructs of mouse full-length Fmn2 (mFmn2 FL) or the nucleation-dead mutant (mFmn2-IA). ***E***, Quantification of protrusion density in Ctl-MO ($n = 44$), Fmn2-MO ($n = 42$, $p = 0.0032$), Fmn2-MO + mFmn2 FL rescue ($n = 42$, $p = 0.0005$), and Fmn2-MO + mFmn2-IA ($n = 39$, $p = 0.7485$) transfected neurons. ***F***, The F-actin patch areas were rescued by morpholino-resistant full-length mouse Fmn2 (mFmn2 FL) but not the morpholino-resistant nucleation-dead mutant (mFmn2-IA). Ctl-MO, $n = 128$; Fmn2-MO, $n = 189$; $p < 0.0001$; Fmn2-MO + mFmn2 FL, $n = 110$; $p = 0.0001$; Fmn2-MO + mFmn2-IA, $n = 156$; $p = 0.7276$. ***G***, ***H***, Representative kymographs depicting the lifespan of F-actin patches in Fmn2-MO + mFmn2 FL (***G***) and Fmn2-MO + mFmn2-IA (***H***) transfected neurons. Arrows mark actin patches and the pink arrow heads mark the "blinking" phenomena of F-actin patches. ***I***, The quantification and comparison of patch lifetime in Ctl-MO ($n = 490$), Fmn2-MO ($n = 693$, $p < 0.0001$), Fmn2-MO + mFmn2 FL ($n = 456$, $p < 0.0001$), and Fmn2-MO + mFmn2-IA ($n = 522$, $p = 0.6537$) transfected neurons. The data are obtained from at least three biological replicates. All the values were plotted with the mean ± SEM indicated. The data were compared using the Kruskal–Wallis test followed by uncorrected Dunn's test; ns, $p > 0.05$, $^{**}p < 0.01$, $^{***}p < 0.001$, $^{****}p < 0.0001$. Scale bar: 10 µm (***C***, ***D***) and 2 µm (***G***, ***H***).

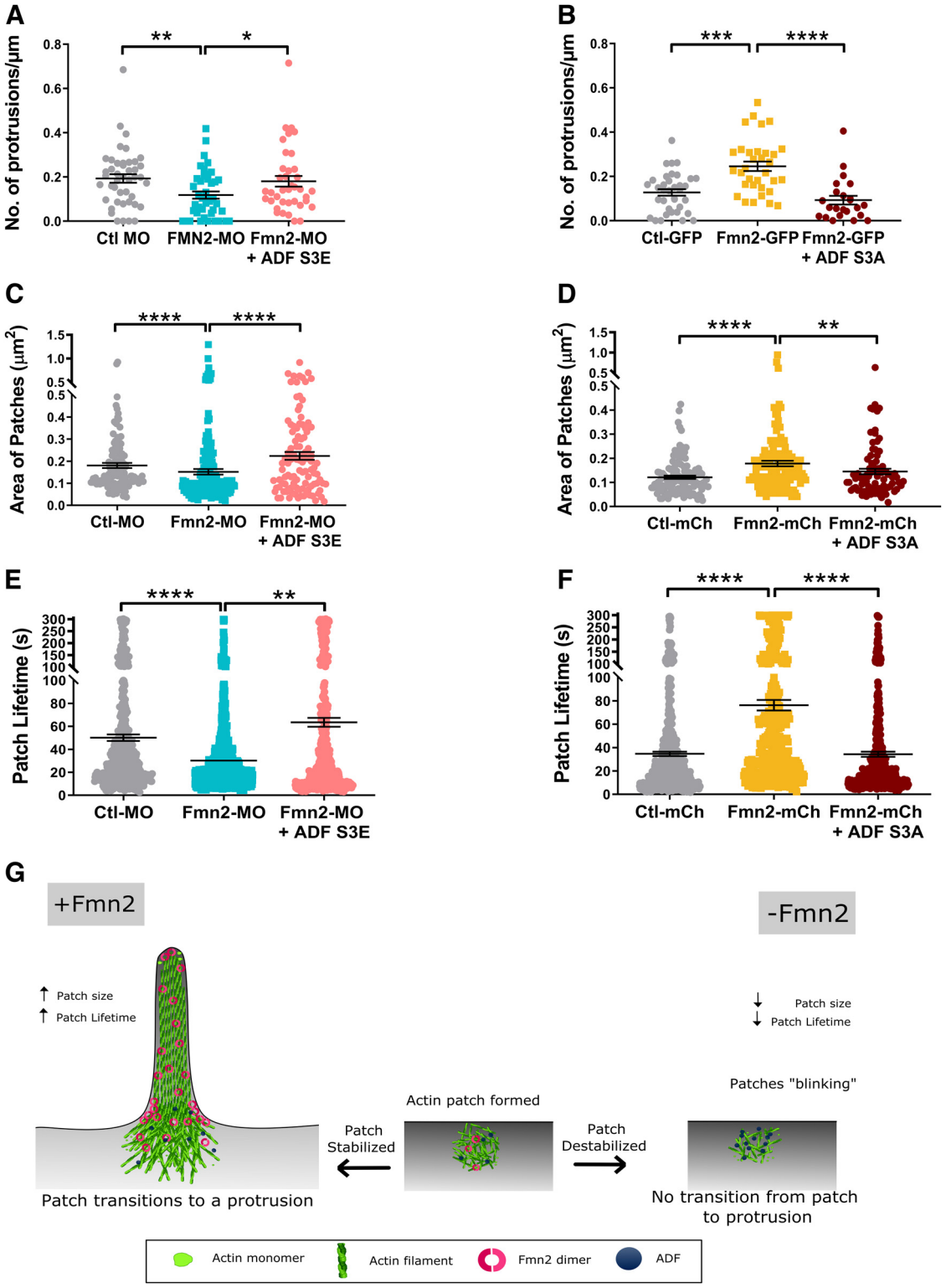

Figure 7. Antagonistic activities of Fmn2 and ADF dynamically regulate axonal protrusions and F-actin patch stability. ***A***, Comparison of axonal protrusion density in Ctl-MO ($n = 44$), Fmn2-MO ($n = 42$, $p = 0.002$), and ADF-S3E ($n = 38$, $p = 0.0482$) transfected neurons. ***B***, Axonal protrusion density in Ctl-GFP-expressing ($n = 36$), gFmn2-GFP-expressing ($n = 33$, $p = 0.0001$), and ADF-S3A + Fmn2 GFP-expressing ($n = 23$, $p < 0.0001$) neurons. ***C***, Comparison of F-actin patch areas in Ctl-MO-treated ($n = 128$), Fmn2-MO-treated ($n = 189$, $p < 0.0001$), and Fmn2-MO + ADF-S3E-treated ($n = 106$, $p < 0.0001$) axons. ***D***, F-actin patch areas in Ctl-mCh-expressing ($n = 121$), Fmn2-mCh-expressing ($n = 125$, $p < 0.0001$), and Fmn2-mCh + ADF S3A-expressing ($n = 86$, $p = 0.0069$) neurons. ***E***, F-actin patch lifetime in Ctl-MO ($n = 490$), Fmn2-MO ($n = 693$, $p < 0.0001$), and ADF-S3E + Fmn2-MO ($n = 483$, $p = 0.0019$) transfected neurons. ***F***, Graphical representation of F-actin patch lifetimes in Ctl-mCh-expressing ($n = 576$), gFmn2-mCh-expressing ($n = 379$, $p < 0.0001$), and ADF-S3A + gFmn2-expressing ($n = 476$; $p < 0.0001$) neurons. ***G***, Model of Fmn2 in F-actin patch dynamics leading to axonal collateral protrusion. An actin patch is initiated by nucleators such as Arp2/3 and/or other formins and is maintained by the activity of Fmn2, which insulates the patch from ADF-mediated depolymerization. Stability of the actin patch renders it competent for signal-induced transition to a nidus of actin polymerization and elongation that initiates a collateral protrusion. On the contrary, in the absence of Fmn2, the actin patch is destabilized by actin severing factors such as ADF, leading to patch

in the axon shaft include the membrane-associated periodic skeleton (MPS), vesicle-associated F-actin "hotspots" and "trails" and collateral branch-inducing focal F-actin patches (Leterrier et al., 2017; Mutalik and Ghose, 2020). The initiation of neurite collateral branching by filopodia-like protrusions generated by F-actin filaments emanating from a focal accumulation of F-actin in the neurite shaft (F-actin patch) is well established in both axons (Gallo, 2006; Orlova et al., 2007; Ketschek and Gallo, 2010; Armijo-Weingart and Gallo, 2017) and dendrites (Nithianandam and Chien, 2018; Stürner et al., 2019). However, the regulation of F-actin patch dynamics remains poorly understood.

Studies in vertebrate sensory neuron axons and fly dendrites have identified WASP-dependent induction of F-actin nucleation by Arp2/3 in initiating the formation of F-actin patches (Spillane et al., 2011; Stürner et al., 2019). The formins are speculated to be involved in filament elongation, though experimental evidence of their involvement in axonal branching is lacking. In this study, we demonstrate that the formin, Fmn2, is a key regulator of F-actin patch dynamics. Fmn2 antagonizes the F-actin depolymerizing activity of ADF to maintain F-actin patches and consequently regulates the initiation of axon collateral branching.

We find that Fmn2 expression is positively correlated with axonal protrusions, and Fmn2 localizes to protrusion-initiating F-actin patches in chick spinal neurons. Depletion of the zebrafish orthologue of Fmn2 also results in a strong reduction in motor neuron branching *in vivo*. The loss of axon collateral branches is seen in both early (22 hpf) and late (48 hpf) stages of motor neuron arborization. However, depletion or overexpression of Fmn2 does not change the number of F-actin patches in axons. This observation indicates F-actin patch formation to be independent of Fmn2 activity. Fmn2 knock-down results in short-lived patches that iteratively disappear, recover and then diminish again at the same location within the axon. This "blinking" phenomenon suggests a role for Fmn2 in F-actin patch maturation or maintenance. It appears that a nucleating core is established independent of Fmn2, however, the maturation and stability of this F-actin network is Fmn2 dependent. This hypothesis is consistent with our observation that F-actin nucleation/polymerization activity of Fmn2 is necessary for its function in F-actin patch dynamics. Overexpression of Fmn2 was found to increase F-actin patch lifetimes, underscoring Fmn2 function in patch stability.

Arp2/3 activity-dependent F-actin patch initiation has been described in multiple systems, including chick sensory neurons, and consistently these networks have a dendritic architecture (Spillane et al., 2011). Thus, it appears Arp2/3, perhaps working in tandem with other actin nucleation promoting factors, is critical for patch formation. However, other activities, including that of Fmn2, is required to aid patch elaboration and maintenance.

Longer-lasting patches are likely to have an increased probability of initiating actin structures required to generate membrane protrusions (Loudon et al., 2006). Comparison of F-actin patch sizes and lifetimes support this hypothesis with patches converting to protrusions being larger and longer-lasting. In fact, the few protrusions that form in axons depleted of Fmn2 also originate from the few remaining patches with longer lifetimes. After facilitating the initiation of protrusions, Fmn2 continues to stay at the base of nascent branches. Our analysis indicates that following maturation and increase in branch length, Fmn2 is no longer located at the branch base. Similarly, recent studies have implicated the development of a dense actin network at the base of nascent branches which resolves once the branch matures (Nedozralova et al., 2022). This suggests a critical role for Fmn2 in initiating branching but it is no longer required at branch bases once the protrusion matures to a branch.

The ADF/cofilin family of F-actin severing and disassembly factors are essential for actin turnover and involved in the dynamics of diverse F-actin networks (Bamburg and Bernstein, 2010; Bernstein and Bamburg, 2010; Kanellos and Frame, 2016). Yeast ADF/Cofilin is a critical component of cortical F-actin patches (Lappalainen and Drubin, 1997; Chen and Pollard, 2013) and recently, loss of ADF/Cofilin activity has been shown to increase axonal branching (Tedeschi et al., 2019). These observations prompted us to directly test whether Fmn2 antagonizes ADF/Cofilin function.

We expressed dominant-negative and constitutively activated mutants of chick ADF, the major ADF/cofilin family member in the chick nervous system (Devineni et al., 1999; Chen et al., 2004), while manipulating Fmn2 expression. Inhibition of ADF activity via the overexpression of dominant-negative ADF in the background of Fmn2 depletion restored the reduction in F-actin patch stability and rescued the deficit in initiating axonal protrusions. Conversely, Fmn2 overexpression induced increased stability of F-actin patches and protrusive activity were both reduced to control levels on co-expression of constitutively-activated ADF. These results strongly implicate antagonistic activities of ADF and Fmn2 in regulating F-actin patch dynamics and, in turn, the initiation of axonal protrusions (Fig. 7*G*). While the exact molecular mechanism of this antagonism remains unknown, recent studies have demonstrated that formin-generated F-actin is resistant to ADF/cofilin-mediate severing both *in vitro* and *in vivo* (Mizuno et al., 2018). As ADF/cofilin activity is ubiquitous in eukaryotic cells, dynamic antagonism by F-actin assembly activities, like that of Fmn2 shown here, is likely to be widespread across phyla in a range of cellular processes.

The actin nucleator Spire, known to function cooperatively with Fmn2 (Vizcarra et al., 2011; Montaville et al., 2014), has been shown to regulate branching in dendritic arbors (Ferreira et al., 2014) though the underlying molecular mechanism has not been elucidated. Taken together with our observations, it is possible that Fmn2 and Spire collaborate to regulate neurite branching in vertebrates. Fmn2 appears to accumulate on the membrane before the appearance of the F-actin patch. Whether this pool of Fmn2 contributes to the initiation of the F-actin patch remains unclear. Subsequently, Fmn2 remains associated with F-actin patch as it elaborates to initiate collateral branching by generating a membrane protrusion.

We propose a dynamic balance of activities, in part involving Fmn2 and ADF, in the maintenance and dynamics of protrusion-competent axonal actin patches (Fig. 7*G*). Resistance to cofilin-induced severing observed in formin-nucleated actin filaments (Mizuno et al., 2018) may have a role in mixed F-actin networks co-regulated by both Arp2/3 and formins, like the axonal F-actin patches. Recent observations from Arp2/3 and formin-induced mixed networks suggest cooperativity where formin-induced filament elongation protects the dense Arp2/3-induced dendritic networks from severing activity of cofilin (Bleicher et al., 2020). In addition to the

←

dissipation without any protrusion initiation. All values were plotted with the mean ± SEM indicated and were obtained from at least three independent experiments. The Kruskal–Wallis test followed by uncorrected Dunn's test for multiple comparisons was used to compare across treatments; $^{*}p < 0.05$, $^{**}p < 0.01$, $^{***}p < 0.0001$, $^{****}p < 0.0001$.

Fmn2-ADF antagonism described here, Fmn2 may regulated F-actin elongation by competing with actin filament capping activities.

Other functionally distinct F-actin networks display different modes of regulation. In the proximal end of the axon, specialized F-actin patches form a selective cargo filter for axonal proteins. However, formin activity is dispensable for these structures and neither does Fmn2 localize to these proximal axon networks in the (Balasanyan et al., 2017). Similarly, Arp2/3-assembled cortical actin patches in yeast are insulated from formins by the activity of capping proteins to maintain a distinct identity (Billault-Chaumartin and Martin, 2019).

In summary, we demonstrate that the neurodevelopmental disorder-associated formin, Fmn2, regulates the maintenance and stability of a specific cytoskeleton network that is critical for the initiation of axon collateral branching. We identify an antagonistic mechanism between Fmn2-mediated F-actin assembly and disassembly by ADF in regulating the dynamics of axonal F-actin patches that are essential for axonal branching.

References

Agís-Balboa RC, Pinheiro PS, Rebola N, Kerimoglu C, Benito E, Gertig M, Bahari-Javan S, Jain G, Burkhardt S, Delalle I, Jatzko A, Dettenhofer M, Zunszain PA, Schmitt A, Falkai P, Pape JC, Binder EB, Mulle C, Fischer A, Sananbenesi F (2017) Formin 2 links neuropsychiatric phenotypes at young age to an increased risk for dementia. EMBO J 36:2815–2828.

Almuqbil M, Hamdan FF, Mathonnet G, Rosenblatt B, Srour M (2013) De novo deletion of FMN2 in a girl with mild non-syndromic intellectual disability. Eur J Med Genet 56:686–688.

Anazi S, et al. (2017) Expanding the genetic heterogeneity of intellectual disability. Hum Genet 136:1419–1429.

Andersen EF, Asuri NS, Halloran MC (2011) In vivo imaging of cell behaviors and F-actin reveals LIM-HD transcription factor regulation of peripheral versus central sensory axon development. Neural Dev 6:27.

Armijo-Weingart L, Gallo G (2017) It takes a village to raise a branch: cellular mechanisms of the initiation of axon collateral branches. Mol Cell Neurosci 84:36–47.

Balasanyan V, Watanabe K, Dempsey WP, Lewis TL Jr, Trinh LA, Arnold DB (2017) Structure and function of an actin-based filter in the proximal axon. Cell Rep 21:2696–2705.

Bamburg JR, Bernstein BW (2010) Roles of ADF/cofilin in actin polymerization and beyond. F1000 Biol Rep 2:62.

Barzik M, McClain LM, Gupton SL, Gertler FB (2014) Ena/VASP regulates mDia2-initiated filopodial length, dynamics, and function. Mol Biol Cell 25:2604–2619.

Bernstein BW, Bamburg JR (2010) ADF/cofilin: a functional node in cell biology. Trends Cell Biol 20:187–195.

Billault-Chaumartin I, Martin SG (2019) Capping protein insulates Arp2/3aAssembled actin patches from formins. Curr Biol 29:3165–3176.e6.

Bleicher P, Sciortino A, Bausch AR (2020) The dynamics of actin network turnover is self-organized by a growth-depletion feedback. Sci Rep 10:6215.

Campbell DS, Stringham SA, Timm A, Xiao T, Law MY, Baier H, Nonet ML, Chien CB (2007) Slit1a inhibits retinal ganglion cell arborization and synaptogenesis via Robo2-dependent and -independent pathways. Neuron 55:231–245.

Chalmers K, Kita EM, Scott EK, Goodhill GJ (2016) Quantitative analysis of axonal branch dynamics in the developing nervous system. PLoS Comput Biol 12:e1004813.

Chen H, Bernstein BW, Sneider JM, Boyle JA, Minamide LS, Bamburg JR (2004) In vitro activity differences between proteins of the ADF/cofilin family define two distinct subgroups. Biochemistry 43:7127–7142.

Chen Q, Pollard TD (2013) Actin filament severing by cofilin dismantles actin patches and produces mother filaments for new patches. Curr Biol 23:1154–1162.

Danzer SC, Crooks KRC, Lo DC, McNamara JO (2002) Increased expression of brain-derived neurotrophic factor induces formation of basal dendrites and axonal branching in dentate granule cells in hippocampal explant cultures. J Neurosci 22:9754–9763.

Dent EW, Barnes AM, Tang F, Kalil K (2004) Netrin-1 and semaphorin 3A promote or inhibit cortical axon branching, respectively, by reorganization of the cytoskeleton. J Neurosci 24:3002–3012.

Devineni N, Minamide LS, Niu M, Safer D, Verma R, Bamburg JR, Nachmias VT (1999) A quantitative analysis of G-actin binding proteins and the G-actin pool in developing chick brain. Brain Res 823:129–140.

Dutta P, Maiti S (2015) Expression of multiple formins in adult tissues and during developmental stages of mouse brain. Gene Expr Patterns 19:52–59.

Dwivedy A, Gertler FB, Miller J, Holt CE, Lebrand C (2007) Ena/VASP function in retinal axons is required for terminal arborization but not pathway navigation. Development 134:2137–2146.

Ferreira T, Ou Y, Li S, Giniger E, van Meyel DJ (2014) Dendrite architecture organized by transcriptional control of the F-actin nucleator Spire. Development 141:650–660.

Flanagan-Steet H, Fox MA, Meyer D, Sanes JR (2005) Neuromuscular synapses can form in vivo by incorporation of initially aneural postsynaptic specializations. Development 132:4471–4481.

Gallo G (2006) RhoA-kinase coordinates F-actin organization and myosin II activity during semaphorin-3A-induced axon retraction. J Cell Sci 119:3413–3423.

Gallo G, Letourneau PC (1998) Localized sources of neurotrophins initiate axon collateral sprouting. J Neurosci 18:5403–5414.

Ganguly A, Tang Y, Wang L, Ladt K, Loi J, Dargent B, Leterrier C, Roy S (2015) A dynamic formin-dependent deep F-actin network in axons. J Cell Biol 210:401–417.

Ghate K, Mutalik SP, Sthanam LK, Sen S, Ghose A (2020) Fmn2 regulates growth cone motility by mediating a molecular clutch to generate traction forces. Neuroscience 448:160–171.

Gibson DA, Ma L (2011) Developmental regulation of axon branching in the vertebrate nervous system. Development 138:183–195.

Gorukmez O, Gorukmez O, Ekici A (2020) A novel nonsense FMN2 mutation in nonsyndromic autosomal recessive intellectual disability syndrome. Fetal Pediatr Pathol 40:702–706.

Kalil K, Dent EW (2014) Branch management: mechanisms of axon branching in the developing vertebrate CNS. Nat Rev Neurosci 15:7–18.

Kanellos G, Frame MC (2016) Cellular functions of the ADF/cofilin family at a glance. J Cell Sci 129:3211–3218.

Katz MJ (1985) Axonal branch shapes. Brain Res 361:70–76.

Kawabata Galbraith K, Kengaku M (2019) Multiple roles of the actin and microtubule-regulating formins in the developing brain. Neurosci Res 138:59–69.

Ketschek A, Gallo G (2010) Nerve growth factor induces axonal filopodia through localized microdomains of phosphoinositide 3-kinase activity that drive the formation of cytoskeletal precursors to filopodia. J Neurosci 30:12185–12197.

Kundu T, Dutta P, Nagar D, Maiti S, Ghose A (2021) Coupling of dynamic microtubules to F-actin by Fmn2 regulates chemotaxis of neuronal growth cones. J Cell Sci 134:jcs252916.

Lappalainen P, Drubin DG (1997) Cofilin promotes rapid actin filament turnover in vivo. Nature 389:211.

Law R, et al. (2014) Biallelic truncating mutations in FMN2, encoding the actin-regulatory protein Formin 2, cause nonsyndromic autosomal-recessive intellectual disability. Am J Hum Genet 95:721–728.

Leader B, Leder P (2000) Formin-2, a novel formin homology protein of the cappuccino subfamily, is highly expressed in the developing and adult central nervous system. Mech Dev 93:221–231.

Lebrand C, Dent EW, Strasser GA, Lanier LM, Krause M, Svitkina TM, Borisy GG, Gertler FB (2004) Critical role of Ena/VASP proteins for filopodia formation in neurons and in function downstream of netrin-1. Neuron 42:37–49.

Leterrier C, Dubey P, Roy S (2017) The nano-architecture of the axonal cytoskeleton. Nat Rev Neurosci 18:713–726.

Loudon RP, Silver LD, Yee HF Jr, Gallo G (2006) RhoA-kinase and myosin II are required for the maintenance of growth cone polarity and guidance by nerve growth factor. J Neurobiol 66:847–867.

Low LK, Cheng HJ (2006) Axon pruning: an essential step underlying the developmental plasticity of neuronal connections. Philos Trans R Soc Lond B Biol Sci 361:1531–1544.

Marco EJ, Aitken AB, Nair VP, da Gente G, Gerdes MR, Bologlu L, Thomas S, Sherr EH (2018) Burden of de novo mutations and inherited rare single

nucleotide variants in children with sensory processing dysfunction. BMC Med Genomics 11:50.

Marler KJ, Becker-Barroso E, Martínez A, Llovera M, Wentzel C, Poopalasundaram S, Hindges R, Soriano E, Comella J, Drescher U (2008) A TrkB/EphrinA interaction controls retinal axon branching and synaptogenesis. J Neurosci 28:12700–12712.

Menon S, Gupton S (2018) Recent advances in branching mechanisms underlying neuronal morphogenesis. F1000Res 7:1779.

Mizuno H, Tanaka K, Yamashiro S, Narita A, Watanabe N (2018) Helical rotation of the diaphanous-related formin mDia1 generates actin filaments resistant to cofilin. Proc Natl Acad Sci U S A 115:E5000–E5007.

Montaville P, Jégou A, Pernier J, Compper C, Guichard B, Mogessie B, Schuh M, Romet-Lemonne G, Carlier MF (2014) Spire and Formin 2 synergize and antagonize in regulating actin assembly in meiosis by a ping-pong mechanism. PLoS Biol 12:e1001795.

Montaville P, Kühn S, Compper C, Carlier MF (2016) Role of the C-terminal extension of formin 2 in its activation by spire protein and processive assembly of actin filaments. J Biol Chem 291:3302–3318.

Mutalik SP, Ghose A (2020) Axonal cytomechanics in neuronal development. J Biosci 45:64.

Nagar D, James TK, Mishra R, Guha S, Burgess SM, Ghose A (2021) The formin Fmn2b is required for the development of an excitatory interneuron module in the zebrafish acoustic startle circuit. eNeuro 8:ENEURO.0329-20.2021.

Nedozralova H, Basnet N, Ibiricu I, Bodakuntla S, Biertumpfel C, Mizuno N (2022) In situ cryo-electron tomography reveals local cellular machineries for axon branch development. J Cell Biol 221:e202106086.

Nithianandam V, Chien CT (2018) Actin blobs prefigure dendrite branching sites. J Cell Biol 217:3731–3746.

Orlova I, Silver L, Gallo G (2007) Regulation of actomyosin contractility by PI3K in sensory axons. Dev Neurobiol 67:1843–1851.

Perrone MD, Rocca MS, Bruno I, Faletra F, Pecile V, Gasparini P (2012) De novo 911 Kb interstitial deletion on chromosome 1q43 in a boy with mental retardation and short stature. Eur J Med Genet 55:117–119.

Quinlan ME, Hilgert S, Bedrossian A, Mullins RD, Kerkhoff E (2007) Regulatory interactions between two actin nucleators, Spire and Cappuccino. J Cell Biol 179:117–128.

Rama S, Zbili M, Debanne D (2018) Signal propagation along the axon. Curr Opin Neurobiol 51:37–44.

Rockland KS (2018) Axon collaterals and brain states. Front Syst Neurosci 12:32.

Roth-Johnson EA, Vizcarra CL, Bois JS, Quinlan ME (2014) Interaction between microtubules and the *Drosophila* formin Cappuccino and its effect on actin assembly. J Biol Chem 289:4395–4404.

Sahasrabudhe A, Ghate K, Mutalik S, Jacob A, Ghose A (2016) Formin 2 regulates the stabilization of filopodial tip adhesions in growth cones and affects neuronal outgrowth and pathfinding in vivo. Development 143:449–460.

Spillane M, Ketschek A, Jones SL, Korobova F, Marsick B, Lanier L, Svitkina T, Gallo G (2011) The actin nucleating Arp2/3 complex contributes to the formation of axonal filopodia and branches through the regulation of actin patch precursors to filopodia. Dev Neurobiol 71:747–758.

Spillane M, Ketschek A, Donnelly CJ, Pacheco A, Twiss JL, Gallo G (2012) Nerve growth factor-induced formation of axonal filopodia and collateral branches involves the intra-axonal synthesis of regulators of the actin-nucleating Arp2/3 complex. J Neurosci 32:17671–17689.

Stürner T, Tatarnikova A, Mueller J, Schaffran B, Cuntz H, Zhang Y, Nemethova M, Bogdan S, Small V, Tavosanis G (2019) Transient localization of the Arp2/3 complex initiates neuronal dendrite branching in vivo. Development 146:dev171397.

Szikora S, Földi I, Tóth K, Migh E, Vig A, Bugyi B, Maléth J, Hegyi P, Kaltenecker P, Sanchez-Soriano N, Mihály J (2017) The formin DAAM is required for coordination of the actin and microtubule cytoskeleton in axonal growth cones. J Cell Sci 130:2506–2519.

Tedeschi A, Dupraz S, Curcio M, Laskowski CJ, Schaffran B, Flynn KC, Santos TE, Stern S, Hilton BJ, Larson MJE, Gurniak CB, Witke W, Bradke F (2019) ADF/cofilin-mediated actin turnover promotes axon regeneration in the adult CNS. Neuron 103:1073–1085.e6.

Vizcarra CL, Kreutz B, Rodal AA, Toms AV, Lu J, Zheng W, Quinlan ME, Eck MJ (2011) Structure and function of the interacting domains of Spire and Fmn-family formins. Proc Natl Acad Sci U S A 108:11884–11889.

Yang C, Svitkina T (2011) Filopodia initiation: focus on the Arp2/3 complex and formins. Cell Adh Migr 5:402–408.